Organic Geochemistry 172 (2022) 104483

Contents lists available at ScienceDirect

Organic Geochemistry

journal homepage: www.elsevier.com/locate/orggeochem

Group 1 phylogeny and alkenone distributions in a freshwater volcanic lake of northeastern China: Implications for paleotemperature reconstructions

Lu Wang [a], Yuan Yao [a,*], Yongsong Huang [b], Yanjun Cai [a], Hai Cheng [a]

[a] Institute of Global Environmental Change, Xi'an Jiaotong University, Xi'an 710054, China
[b] Department of Earth, Environmental and Planetary Sciences, Brown University, Providence, RI 02912, USA

ARTICLE INFO

Associate Editor–Liz Minor

Keywords:
Group 1 Isochrysidales
Alkenone isomers
Paleotemperature proxies
Freshwater lakes

ABSTRACT

Long-chain alkenones (LCAs) produced by Group 1 Isochrysidales from freshwater lakes feature a highly specific profile with almost the same abundances of two C_{37} tri-unsaturated alkenone isomers. Their unsaturation ratios have been proposed to have great potential for cold-season paleotemperature reconstructions. However, recent study based on the next-generation sequencing has found that there is high level of genetic diversity in Group 1 Isochrysidales, with two main subclades Groups 1a and 1b. It is still unclear whether variable mixtures of different Group 1 subclades can significantly affect the LCA-based paleotemperature proxies in freshwater lake sediment records. Here we investigated LCA distributions and haptophyte-specific 18S rRNA sequences from a sediment core in Tuofengling Tianchi (a freshwater volcanic lake) of northeastern China using a combination of lipid biomarker and next-generation sequencing analyses. We recover 386 amplicon sequence variants (ASVs) from the studied sediment samples, 11 of which are affiliated with the LCA-producing Isochrysidales. Our phylogenetic analysis identifies that all LCA-producing Isochrysidales belong to Group 1 phylotype (Groups 1a and 1b subclades included), with Group 1a being the dominant subclade in most samples. The phylotype is strongly supported by the LCA evidence of two C_{37} tri-unsaturated alkenone isomers, with RIK_{37} (ratio of isomeric ketones of C_{37} chain length) of ~ 0.57–0.60. Groups 1a and 1b in our sediment core display significant downcore variations in the relative abundances, with Group 1a ranging from 32% to 100%. However, such highly variable mixtures are not a dominant factor in affecting the values of LCA-based on temperature proxies (U^K_{37}, U^K_{38}Et, and R3b) in our sediment core. Our study provides the sedimentary evidence that Group 1 LCAs elude species-mixing effects and highlight the potential importance of Group 1 LCAs from freshwater lakes in quantitatively reconstructing past temperature changes.

1. Introduction

Long-chain alkenones (LCAs) are a series of C_{35}–C_{42} methyl or ethyl ketones with 2–4 double bonds which are produced by certain Isochrysidales algae within haptophyte lineages. They have been found to extensively occur in the world's oceans (e.g., Marlowe et al., 1990; Conte et al., 2006) and various lake environments (e.g., Zink et al., 2001; Chu et al., 2005; Pearson et al., 2008; Toney et al., 2010; Longo et al., 2016, 2018; Plancq et al., 2018; Yao et al., 2019, 2022; Sawada et al., 2020). Based on haptophyte phylogenetic analysis, numerous studies have divided LCA-producing Isochrysidales into three groups: Group 1 thriving in freshwater lakes, Group 2 in brackish/coastal marine environments, and Group 3 in open marine environments (Theroux et al., 2010; D'Andrea et al., 2016; Longo et al., 2016; Kaiser et al., 2019; Plancq et al., 2019; Yao et al., 2019). Group 1 Isochrysidales contain two main subclades: Groups 1a and 1b (Richter et al., 2019), but their species/strains have not been successfully isolated for laboratory culture. Group 2 Isochrysidales have recently been divided into three main subclades: Groups 2i, 2w1 and 2w2 (Yao et al., 2022), and include named species *Ruttnera* (*Chrysotila*) *lamellosa*, *Isochrysis galbana*, *Isochrysis litoralis* and *Isochrysis nuda* (e.g., Sun et al., 2007; Nakamura et al., 2014; Zheng et al., 2016, 2019; Liao et al., 2020). Group 3 Isochrysidales include two named species *Emiliania huxleyi* and *Gephyrocapsa oceanica* (Volkman et al., 1980, 1995; Sawada et al., 1996; Conte et al., 1998) with high genetic similarity.

The unsaturation ratios of LCAs (U^K_{37} and $U^{K'}_{37}$) are important tools for paleotemperature reconstructions, with higher degree of unsaturation corresponding to lower temperature. These proxies have been exten-

* Corresponding author.
E-mail address: yaoyuan@xjtu.edu.cn (Y. Yao).

https://doi.org/10.1016/j.orggeochem.2022.104483
Received 5 May 2022; Received in revised form 6 August 2022; Accepted 11 August 2022
Available online 13 August 2022

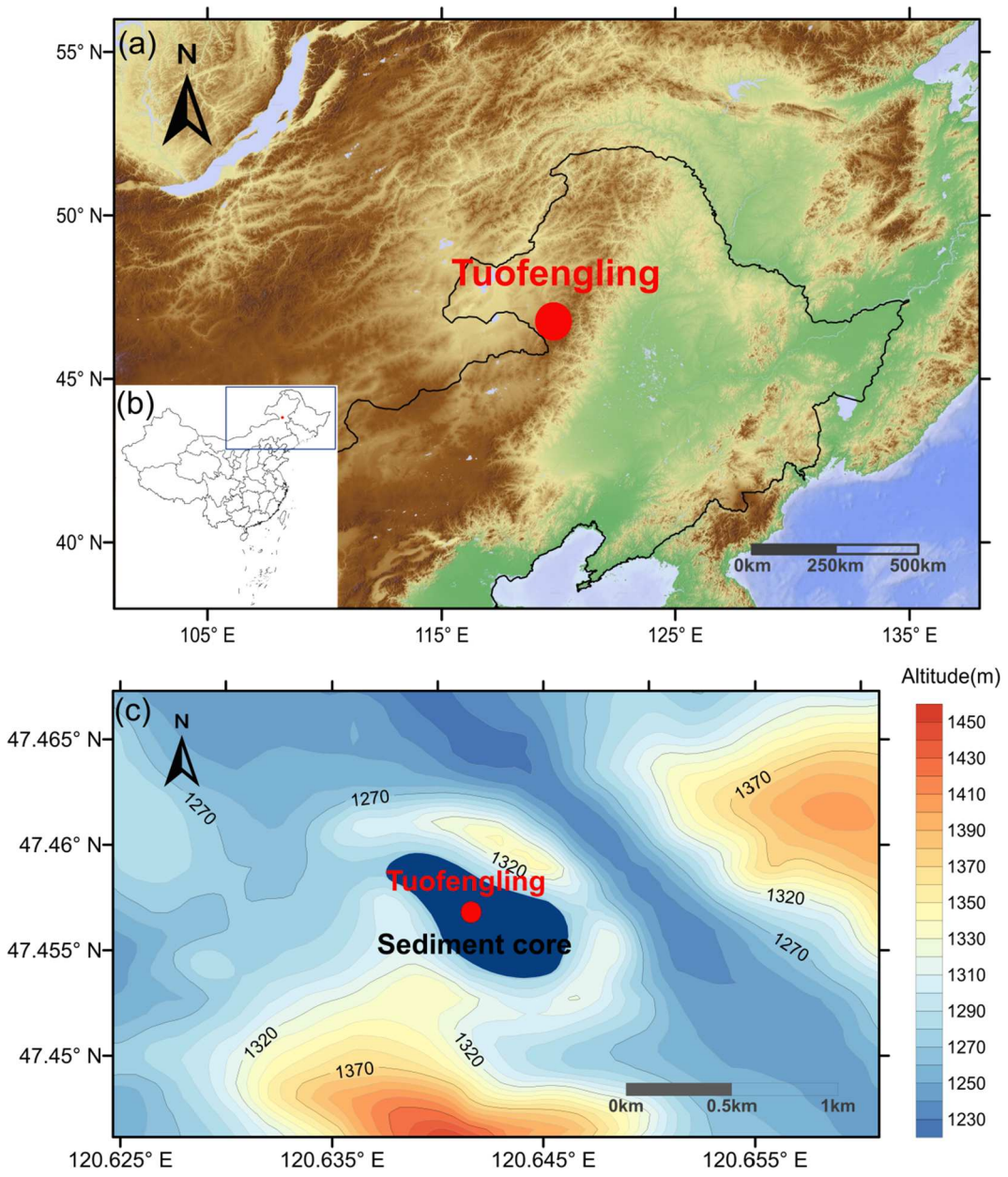

Fig. 1. (a, b) The geographical location of Tuofengling Tianchi in this study. (c) Contour map showing the location of Tuofengling Tianchi sediment core and the surrounding geographic information.

sively and successfully used to reconstruct past sea surface temperatures in numerous paleoclimatic and paleo-oceanographic studies (e.g., Brassell et al., 1986; Prahl and Wakeham, 1987; Eglinton et al., 1992). However, compared to open marine environments, saline lakes harbor multiple LCA-producing Group 2 species/subclades, with different temperature sensitivities and growth seasons (Theroux et al., 2010, 2020; Yao et al., 2022). In particular, the Group 2i subclade blooms in spring, whereas Groups 2w1 and 2w2 bloom in summer (Theroux et al., 2020; Yao et al., 2022). This creates significant difficulties in widespread applications of U^{K}_{37} and $U^{K'}_{37}$ for continental paleotemperature reconstructions.

In freshwater lakes, LCAs produced by Group 1 Isochrysidales have been proposed to have great potential for quantitative continental paleotemperature reconstructions (Longo et al., 2016, 2018; Yao et al., 2019). They have maximum production during lake ice melt and isothermal mixing (D'Andrea et al., 2011, 2016; Longo et al., 2018) and mainly record cold season temperature signals (Longo et al., 2018; Yao et al., 2019). The Group 1 LCAs contains a series of specific tri-unsaturated isomers (such as $C_{37:3b}$ and $C_{38:3b}$Et) that are absent in Groups 2 and 3 Isochrysidales (Longo et al., 2013, 2016; Zheng et al., 2019). Based on the ratios of tri-unsaturated isomers, RIK_{37} and RIK_{38E} (ratios of isomeric ketones; RIK) indices have been proposed as chemotaxonomic indicators for input of Group 1 Isochrysidales in lake sediments (Longo et al., 2016), and have been successfully applied to the sedimentary records from two oligohaline lakes of China (Yao et al., 2020, 2021) and Black Sea (Huang et al., 2021). Previous studies using the haptophyte-specific primers from Coolen et al. (2004) for the targeted DNA amplification have found that Group 1 Isochrysidales include a limited number of dominant genotypes in globally distributed freshwater lakes (Theroux et al., 2010; D'Andrea et al., 2016; Plancq et al., 2018; Yao et al., 2019; Wang et al., 2019a). However, using next-generation sequencing with a pair of universal eukaryote and haptophyte-specific primers (Egge et al., 2013), Richter et al. (2019) found high levels of genetic diversity in Group 1 Isochrysidales from

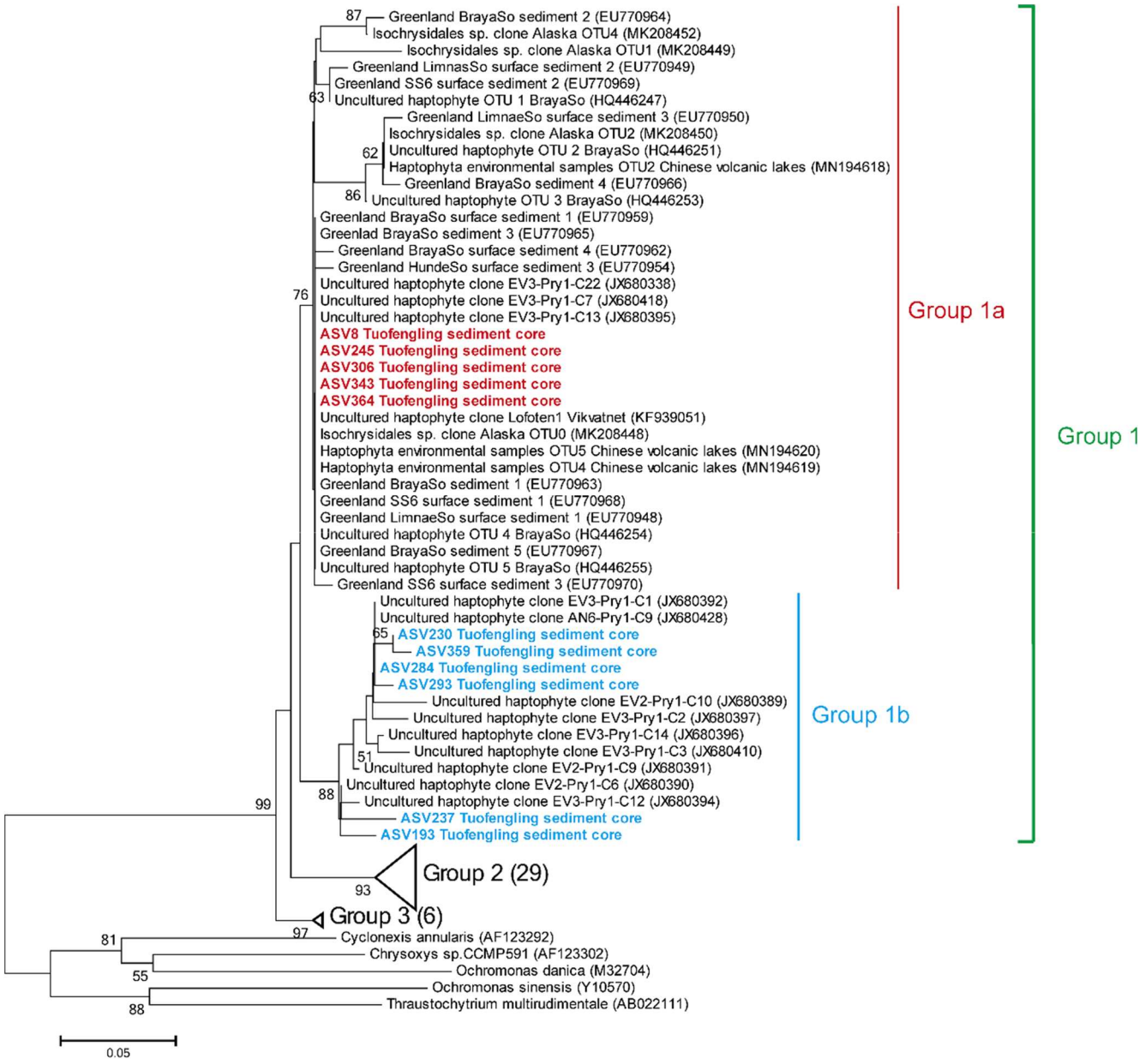

Fig. 2. Consensus neighbor-joining phylogenetic tree depicting 18S rRNA gene-inferred relatedness of haptophytes. Groups 2 and 3 are shown collapsed. Bootstrap values greater than 50% are shown at nodes.

some freshwater lakes in Alaska, Iceland and Germany, with two main subclades Group 1a (S-Oligotypes 1a) and Group 1b (S-Oligotypes 1b). This raises a critical question: can variable mixtures of different Group 1 subclades in lake sedimentary records significantly affect Group 1 LCAs-based paleotemperature proxies?

In a series of freshwater volcanic lakes in northeastern China, Yao et al. (2019) have demonstrated the widespread occurrence of Group 1 LCAs. Here, we collected a short sediment core from Group 1 LCA-containing Tuofengling Tianchi (a freshwater volcanic lake; Yao et al., 2019) of northeastern China, and used a paired analysis of lipid biomarker and next-generation sequencing to determine the downcore LCA distributions and haptophyte 18S rRNA. Our main objectives are to: (1) classify phylogenetically Group 1 subclades in the sediment core samples, and (2) verify whether temperature proxies based on Group 1 LCAs are not affected by the mixing effects of different Group 1 genotypes.

2. Materials and methods

2.1. Study sites and samples

Tuofengling Tianchi (47°27′N; 120°38′E; ~1100 m a.s.l.) is located in the Arxan-Chaihe volcano area on the Greater Khingan Mountains of northeast China (Fig. 1). It is currently a freshwater crater lake (salinity measured on July 2016 is 0.02 ppt; Yao et al., 2019) with the maximum water depth of ~30 m and lake area of 0.23 km^2 (Yao et al., 2019). The region lies on the northern boundary of the modern East Asian Summer Monsoon (EASM). The modern climate is characterized by strong seasonality, with a warm and humid summer and a cold and dry winter. The mean annual air temperature (MAAT; 1979–2013) is about –2.6 °C, the mean annual precipitation is 440 mm (MAP; 1970–2013; Karger et al., 2017).

We collected a 38 cm sediment core from Tuofengling Tianchi at a water depth of ~15 m in July 2017 (Fig. 1b). The core above 28 cm was

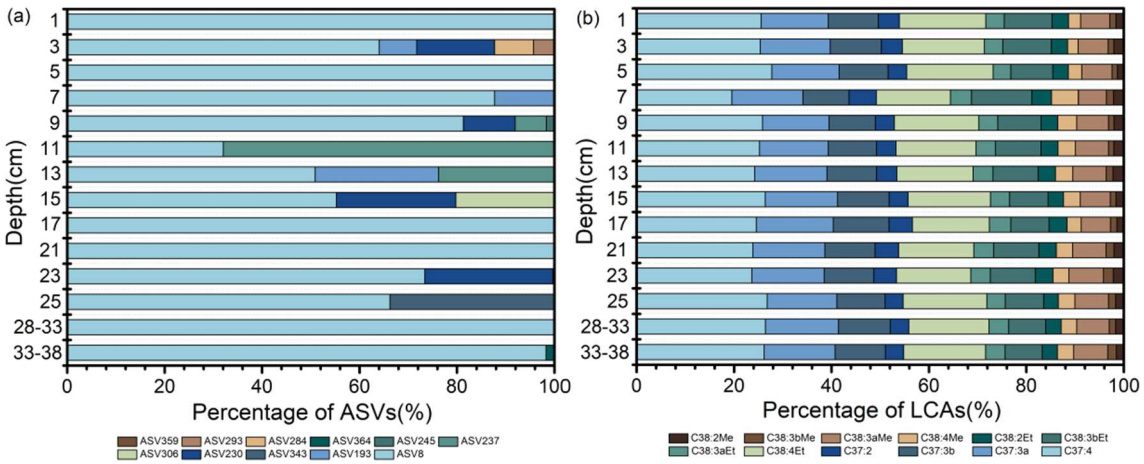

Fig. 3. (a) The relative abundances of ASVs and (b) LCAs from our Tuofengling Tianchi sediment core along depth variation.

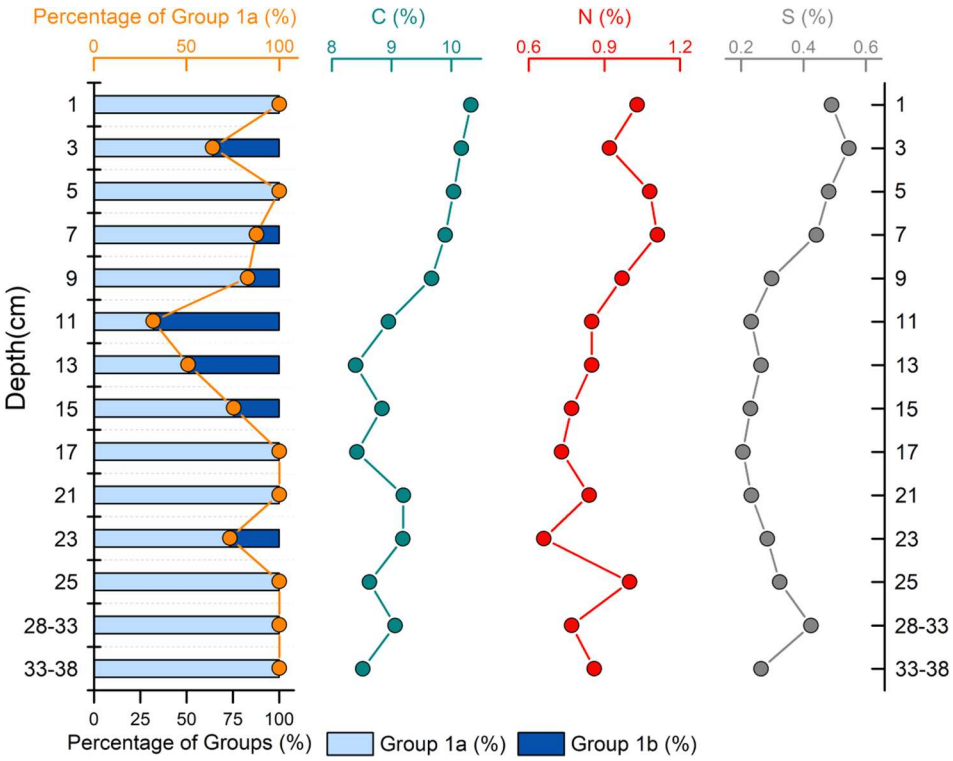

Fig. 4. The relative abundances of Groups 1a and 1b DNA sequences and total C, N, S from our Tuofengling Tianchi sediment core along depth variation.

sub-sampled at 1 cm intervals, and the samples below 28 cm were sub-sampled at 5 cm intervals. All samples were analyzed for LCA analysis, and 16 samples were selected for DNA analysis. The sediment samples for DNA analysis were frozen at –80 °C and the sediment samples for LCA analysis were frozen at –20 °C in the laboratory.

2.2. Methods

2.2.1. DNA analysis

DNA of 16 sediment core samples was extracted using the FastDNA® Spin Kit for Soil (MP Biomedicals, USA) according to manufacturer's instructions. The DNA extract was checked on 1% agarose gel, and DNA concentration and purity were determined with NanoDrop 2000 UV–vis spectrophotometer (Thermo Scientific, Wilmington, USA). The hyper-variable region V4 of the haptophyte 18S rRNA gene were amplified using a primer pair (universal eukaryote forward primer 528Flong: 5'-GCGGTAATTCCAGCTCCAA-3' and haptophyte-specific reverse primer PRYM01+7: 5'-GATCAGTGAAAACATCCCTGG-3' (Egge et al., 2013)) by an ABI GeneAmp® 9700 PCR thermocycler (ABI, CA, USA). The PCR amplification of 18S rRNA gene was performed as follows: initial denaturation at 95 °C for 3 min, followed by 40 cycles of denaturing at 95 °C for 30 s, annealing at 60 °C for 30 s and extension at 72 °C for 45 s, and single extension at 72 °C for 10 min, and end at 10 °C. The PCR mixtures contain 4 μl 5 × FastPfu buffer, 2 μl 2.5 mM dNTPs, 0.8 μl forward primer (5 μM), 0.8 μl reverse primer (5 μM), 0.4 μl FastPfu polymerase, 0.2 μl BSA, 10 ng template DNA, and finally ddH_2O (double distilled H_2O) up to 20 μl. PCR reactions were performed in triplicate. The PCR product was extracted from 2% agarose gel and purified using the AxyPrep DNA Gel Extraction Kit (Axygen Biosciences, Union City, CA, USA) according to the manufacturer's instructions and quantified using a Quantus™ fluorometer (Promega, USA). Purified amplicons were pooled in equimolar and paired-end sequenced on an Illumina

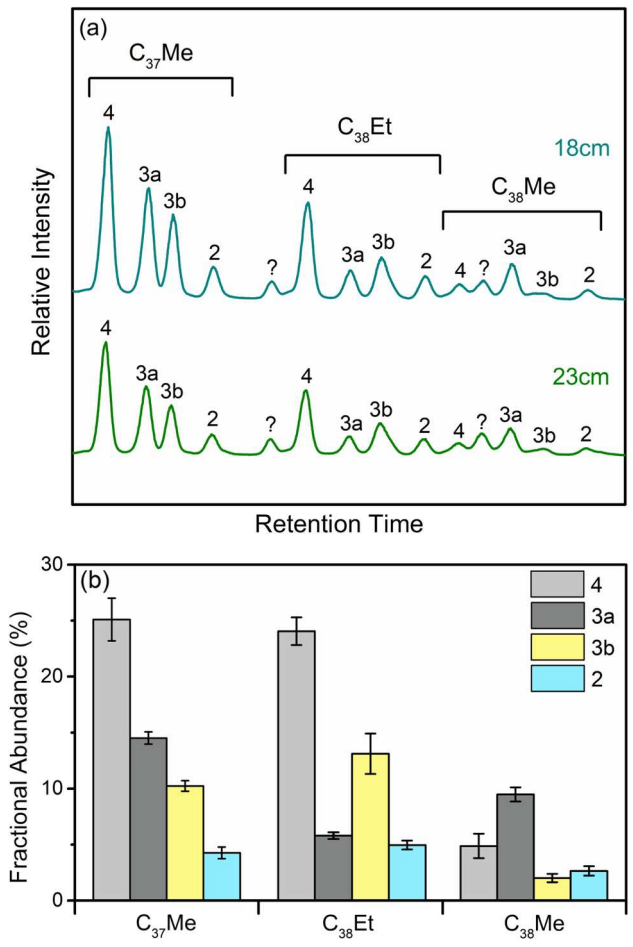

Fig. 5. (a) Partial gas chromatograms of LCAs from Tuofengling Tianchi sediment core at the depth of 18 cm and 23 cm. (b) Average fractional abundances of LCAs in all Tuofengling Tianchi sediment core samples.

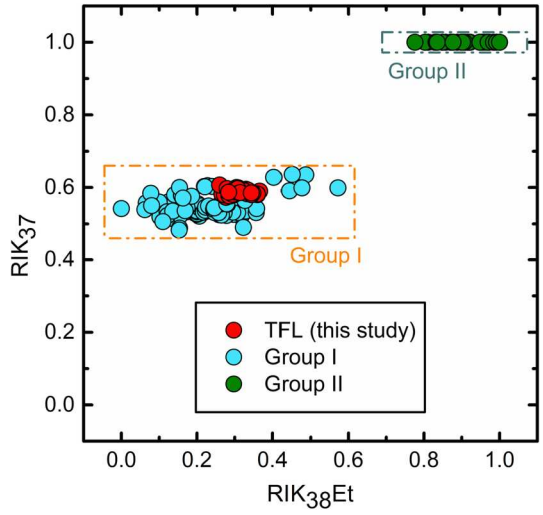

Fig. 6. RIK_{37} and $RIK_{38}Et$ indices distinguish Group 1 from Group 2 LCAs. Red circles represent the LCA data from our Tuofengling Tianchi sediment core, light blue circles represent the published Group 1 LCA data (Longo et al., 2016, 2018; Yao et al., 2019), and green circles represent the published Group 2 LCA data (Nakamura et al., 2014; Araie et al., 2018; Zheng et al., 2019; Liao et al., 2020). (For interpretation of the references to colour in this figure legend, the reader is referred to the web version of this article.)

MiSeq PE300 platform (Illumina, San Diego, USA).

After demultiplexing, the resulting sequences were merged with FLASH (v1.2.11) (Magoč and Salzberg, 2011) and quality filtered with fastp (0.19.6) (Chen et al., 2018). Then the high-quality sequences were de-noised using DADA2 (Callahan et al., 2016) plugin in the Qiime2 (version 2020.2) (Bolyen et al., 2019) pipeline with recommended parameters, which obtains single-nucleotide resolution based on error profiles within samples. DADA2 denoised sequences are usually called amplicon sequence variants (ASVs). Taxonomic assignment of ASVs was performed using the Blast consensus taxonomy classifier implemented in Qiime2 and the SILVA reference database.

2.2.2. LCAs analysis

The samples for LCAs analysis were freeze-dried and were extracted three times by sonication with dichloromethane (DCM)/methanol (MeOH) (9:1, v/v). The total lipid extracts were then separated by column chromatography with silica gel using *n*-hexane, DCM, and MeOH, respectively. The DCM fractions were further purified by column chromatography with silver thiolate silica (Wang et al., 2019b). Using a sequence of solvents (hexane/DCM (4:1, v/v, 2 ml), acetone (2 ml)) with increasing polarity, all LCA compounds were eluted in the acetone fractions. All LCAs were analyzed using an Agilent 8890 GC system with a flame ionization detector (FID) and a Restek Rtx-200 GC column (105 m × 250 μm × 0.25 μm) at Xi'an Jiaotong University, China. Helium was used as the carrier gas, and the column flow rate was 1.5 ml/min. The following GC-FID oven program was used: initial temperature of 50 °C (hold 2 min), ramp 20 °C/min to 255 °C, ramp 3 °C/min to 310 °C (hold 30 min).

The LCA indices U^K_{37} (Brassell et al., 1986), $U^K_{38}Et$ ("Et" refers to ethyl ketone), R3b (Longo et al., 2018), RIK_{37} and $RIK_{38}Et$ (Longo et al., 2016) were calculated as follows:

$$U^K_{37} = \frac{C_{37:2} - C_{37:4}}{C_{37:2} + (C_{37:3a} + C_{37:3b}) + C_{37:4}} \quad (1)$$

$$U^K_{38}Et = \frac{C_{38:2}Et - C_{38:4}Et}{C_{38:2}Et + (C_{38:3a}Et + C_{38:3b}Et) + C_{38:4}Et} \quad (2)$$

$$R3b = \frac{[C_{37:3b}]}{[C_{38:3b}Et + C_{37:3b}]} \quad (3)$$

$$RIK_{37} = \frac{[C_{37:3a}]}{[C_{37:3a} + C_{37:3b}]} \quad (4)$$

$$RIK_{38}Et = \frac{[C_{38:3a}Et]}{[C_{38:3a}Et + C_{38:3b}Et]} \quad (5)$$

where the "a" and "b" subscripts refer to the Δ7,14,21 and Δ14,21,28 triunsaturated LCAs, respectively.

2.2.3. Element and radiocarbon analysis

The contents of three major elements (C, N, and S) in 14 samples were detected by the CHNS mode of the Vario EL Cube elemental analyzer. The samples were catalytically oxidized in a high temperature and oxygen-rich environment, and the combustion produces CO_2, N_2, SO_2, CO and other gases. The generated gas mixture was separated by gas chromatography and quantified using a thermal conductivity detector after eliminating interferences. Helium was used as carrier gas and purge gas, and the oxygenation time was 80 s. Two sets of standards were measured, and the standard deviations of C, N, and S were less than 0.001%.

Total organic carbon (TOC) of two sediment samples at the depths of 28 cm and 38 cm was measured for radiocarbon dating by acceleration mass spectrometry (AMS) at Xi'an AMS Center, China.

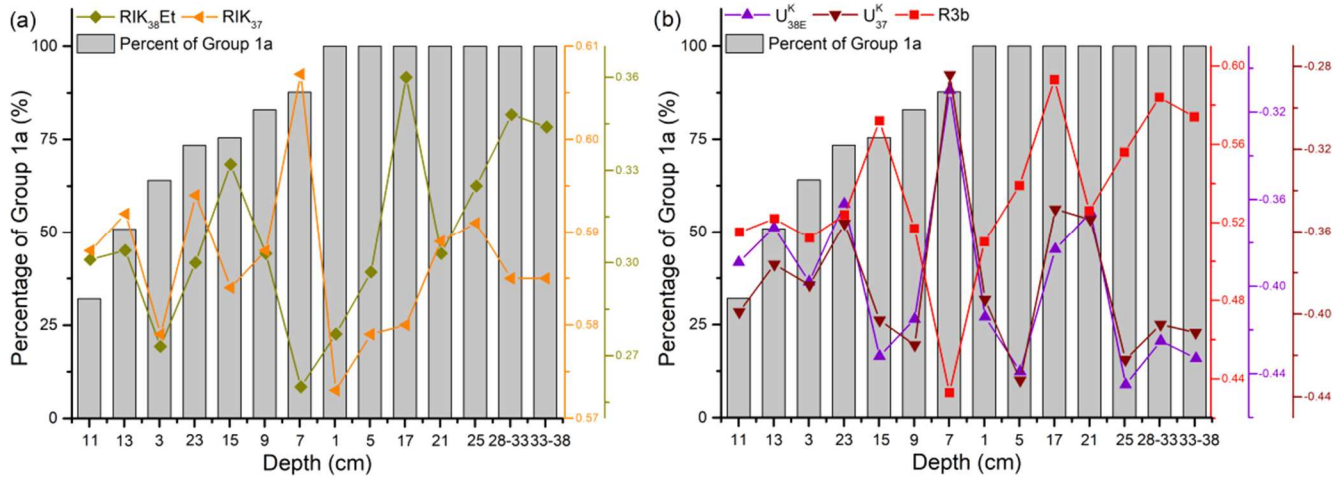

Fig. 7. Relative abundance of Group 1a DNA sequences (relative to total Group 1 DNA sequences) vs RIK_{37}, $RIK_{38}Et$, U^K_{37}, $U^K_{38}Et$, and R3b in our Tuofengling Tianchi sediment core samples.

3. Results and discussion

3.1. 18S rRNA-based Isochrysidales identification and phylogenetic classifications

We selected 16 sediment samples of our sediment core for PCR amplification using the primers described in Egge et al. (2013), and all samples yielded positive amplification with the targeted DNA band productions (Supplementary Fig. S1). We sequenced the 18S rRNA sequences from the 16 samples using next-generation sequencing (Supplementary Table S1). A total of 386 amplicon sequence variants (ASVs) were recovered from all the samples studied (Supplementary Table S1). Among them, 366 ASVs belong to the Eukaryota and 20 ASVs do not correspond to any known sequences referenced within the SILVA database. Of the 366 ASVs within the Eukaryota, 11 ASVs belong to the LCA-producing Isochrysidales (ASV8, 193, 343, 230, 306, 237, 245, 364, 284, 293, 359; Supplementary Table S2). However, two sediment samples (TFL19 and TFL27) did not contain the 11 LCA-producing Isochrysidales ASVs despite positive PCR amplification (Supplementary Table S2). This may be due to very low relative abundance of Isochrysidales DNA compared with the total targeted Eukaryota in the two samples.

We reconstructed a phylogenetic tree using the 11 ASVs of the LCA-producing Isochrysidales along with 69 Isochrysidales DNA sequences from the NCBI GenBank database (Fig. 2). We divided Group 1 Isochrysidales into two phylogenetically distinct clades Group 1a and Group 1b based on our phylogenetic tree, which are supported respectively by 76% and 88% bootstrap values (Fig. 2). All of 11 ASVs are affiliated with Group 1 Isochrysidales. 5 ASVs (ASV8, ASV245, ASV306, ASV343, and ASV364) belong to the Group 1a clade, and 6 ASVs (ASV284, ASV230, ASV359, ASV293, ASV237, and ASV193) belong to the Group 1b clade.

Using the primers from Coolen et al. (2004) for the Isochrysidales DNA amplification, Group 1a (formerly "Greenland" subclade; D'Andrea et al., 2006) has been found to extensively occur in globally distributed freshwater lakes, including Greenland (D'Andrea et al., 2006), Canada (Theroux et al., 2010), Norway (D'Andrea et al., 2016), Japan (Plancq et al., 2018), northeastern China (Yao et al., 2019), and Alaska (Wang et al., 2019a). However, due to primer mismatch, Simon et al. (2013) only amplified Group 1b (formerly "EV" subclade) from the investigated freshwater lakes in France. Importantly, recent studies (Plancq et al., 2019; Richter et al., 2019) have found that both Group 1a and Group 1b clades can be recovered using another pair of different primers from Egge et al. (2013) and next-generation sequencing.

Here we also found the occurrence of both Group 1a and Group 1b clades in our sediment core using the primers from Egge et al. (2013) (Fig. 2). Our next-generation sequencing yield high phylogenetic diversity in Group 1 Isochrysidales, with 11 Group 1 ASVs. In most of our samples, Group 1a, especially ASV8, is the dominant clade (Fig. 3a). In particular, the samples of 1, 5, 17, 21, 28–33 cm depth only contain Group 1a ASV8 based on our recovered DNA sequences. ASV abundances display significant downcore variations, but LCA distributions have no obvious changes along the depth (Fig. 3). The relative abundance of Group 1a generally decreases from the surface sediment to the depth of 11 cm, followed by an overall increase with increasing depth, which is not consistent with changes in major element C, N, and S (Fig. 4).

3.2. LCA distributions in sediment core

Our sediment core spans ~980 years based on two ^{14}C ages (Supplementary Table S3). We analyzed LCA distributions from 30 sediment samples of our sediment core, and all samples contain abundant C_{37} and C_{38} alkenones (Fig. 5b). C_{37} alkenones have the highest abundance, accounting for more than 50%, followed by $C_{38}Et$ and $C_{38}Me$ alkenones. The distributions of LCAs are highly consistent in all samples (Fig. 3b and 5b) and display the characteristics of Group 1-type alkenones, with the presence of the tri-unsaturated isomer $C_{37:3b}$ and $C_{38:3b}Et$, as well as $C_{38}Me$ (Fig. 5a; Longo et al., 2016).

RIK_{37} and $RIK_{38}Et$ have been proposed as taxonomic indicators for the relative contribution of Group 1 Isochrysidales, with 0.51–0.60 for RIK_{37} and 0.1–0.6 for $RIK_{38}Et$ indicating dominant Group 1 (Longo et al., 2016, 2018). The reliability of the proxies has been further verified by Yao et al. (2019) by a combination of 18S rRNA and LCA distributions in freshwater volcanic lakes of northeastern China. We followed the approach from Longo et al. (2018) to differentiate Group 1 alkenones from Group 2 using RIK_{37} and $RIK_{38}Et$ (Fig. 6). To evaluate more reliably the chemotaxonomic classification, we used more alkenone data, including 104 Group 1 alkenone data (Supplementary Table S3; Longo et al., 2016, 2018; Yao et al., 2019) and 98 Group 2 alkenone data (Supplementary Table S4; Nakamura et al., 2014; Araie et al., 2018; Zheng et al., 2019; Liao et al., 2020). In our sediment core samples, RIK_{37} ranges from 0.573 to 0.607 with an average value of 0.587, and $RIK_{38}Et$ ranges from 0.260 to 0.366 with an average value of 0.310 (Fig. 6). All samples fall within the proposed range of Group 1 LCAs (Fig. 6), indicating that the LCAs of our sediment core are produced predominantly by Group 1 Isochrysidales. This is further supported by our 18S rRNA results (Figs. 2 and 3a).

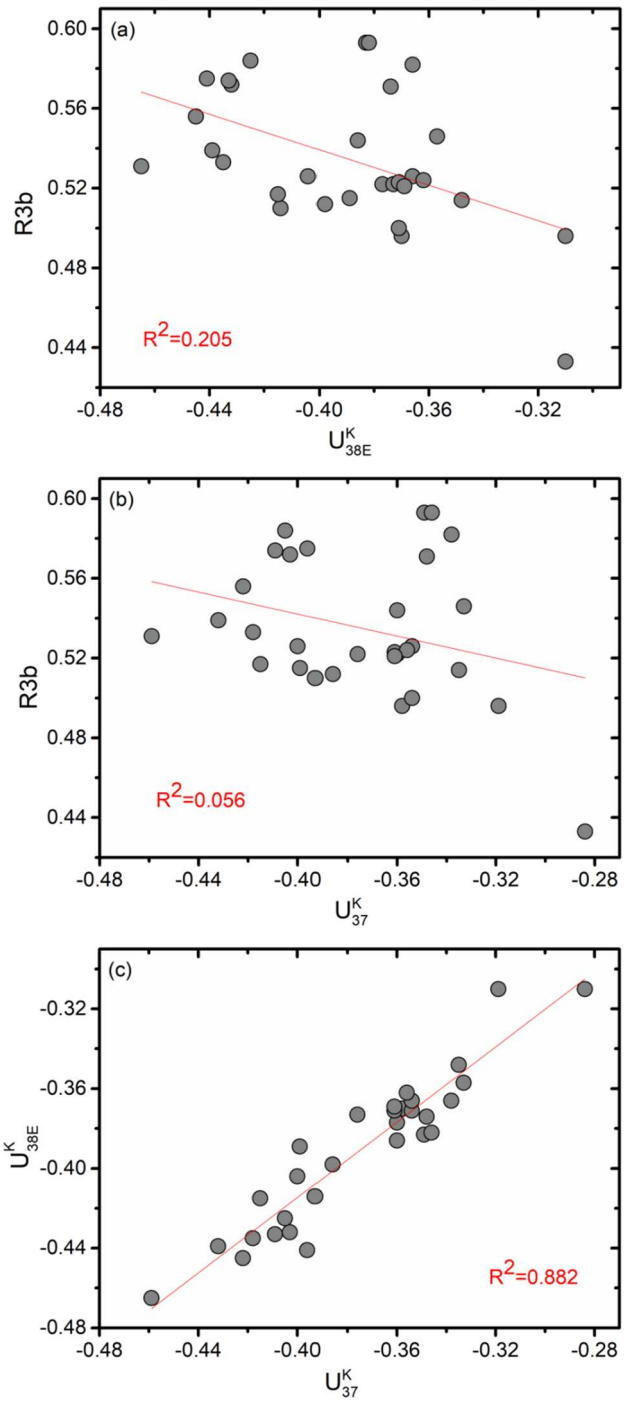

Fig. 8. Correlations among three alkenone temperature indices (U^K_{37}, U^K_{38}Et, and R3b) in our Tuofengling Tianchi sediment core samples.

3.3. The LCA indices and Group 1 subclades

In addition to RIK_{37} and RIK_{38}Et as taxonomic proxies (Longo et al., 2016, 2018), Group 1 U^K_{37}, U^K_{38}Et, and R3b have been proposed as temperature proxies for cold-season temperature reconstructions (Longo et al., 2018; Yao et al., 2019). Especially in the sediments with mixed Groups 1 and 2 LCAs, R3b still reflects the cold-season temperature signal from Group 1, because $C_{37:3b}$ and $C_{38:3b}$Et likely have no contributions from Group 2 producers (Longo et al., 2018). However, it is still unclear whether variable mixtures of different Group 1 subclades can significantly affect these proxies.

Previous studies have hypothesized that Group 1 alkenones may not be affected by species-mixing effects, mainly due to the general consistency of the responses of Group 1 alkenones to temperature changes as seen in lake suspended particulate matter (SPM) and surface sediments of Northern Hemispheric freshwater lakes (Longo et al., 2016, 2018). In our sediment core samples, the distributions of LCAs show high consistency with depth (Fig. 3b), despite high diversity in DNA ASVs and their variable changes (Fig. 3a). The two main subclades Groups 1a and 1b also display significant downcore variations (Fig. 4). We plotted two figures showing the changes in alkenone indices, including RIK_{37}, RIK_{38}Et, U^K_{37}, U^K_{38}Et, and R3b, against the relative abundance of Group 1a (Fig. 7). We find that the changes in these alkenone indices do not respond to increasing Group 1a abundance (Fig. 7), and there are poor correlations between Group 1a abundance and the five alkenone indices (Supplementary Fig. S2). Thus, we suggest that the shifts in Groups 1a and 1b may not be the dominant factor in affecting the values of these alkenone indices in our sediment core.

Recent study has found that the relative abundances of Groups 1a and 1b are highly variable in northern Alaskan lake water samples at different sampling depths and times (Richter et al., 2019). However, the U^K_{37}, U^K_{38}Et, and R3b values of SPM samples from these Alaskan lakes are still strongly correlated with in situ water temperatures (Longo et al., 2016, 2018; Supplementary Fig. S3). These results, together with our sediment core data, provide evidence that Group 1 alkenones may be unaffected by the species-mixing effects. We suggest that the alkenone distributions from the two main subclade Group 1a and Group 1b may have similar behaviors in response to temperature changes. Future studies focused on the isolation and culturing of Group 1 subclades would provide further evidence of their response to ecological conditions.

3.4. Correlations among alkenone temperature proxies

Group 1 alkenone-producing Isochrysidales have been demonstrated to bloom during the spring transitional season in various freshwater lakes (D'Andrea et al., 2011, 2016; Longo et al., 2018; Richter et al., 2019). The lake water temperatures at that time are dependent on lake ice thickness in the winter and spring and the timing of spring thaw (Longo et al., 2018; Yao et al., 2019), which is primarily affected by winter-spring air temperature changes (Longo et al., 2020; Richter et al., 2021). The colder winter-spring air temperatures can result in thicker lake ice, which exerts lasting effects on the spring lake temperatures through the duration of ice melt and the delaying of late-spring (or summer) lake surface warming (Longo et al., 2020). Although U^K_{37}, U^K_{38}Et, and R3b values of SPM samples from the northern Alaska freshwater lakes have good correlations with in situ lake water temperatures (Longo et al., 2016, 2018; Supplementary Fig. S3), they display different behaviors in surface sediments from Northern Hemispheric freshwater lakes in response to seasonal temperature changes (Yao et al., 2019). The U^K_{37} and U^K_{38}Et well reflect the changes in mean air temperature of the spring isothermal season (Longo et al., 2018; Yao et al., 2019), whereas in the relatively warm regions with the mean winter temperature higher than ~–20 °C, R3b appears to more sensitive to winter air temperature changes (Yao et al., 2019). This may be associated with lake ice thickness controlled by winter temperatures and associated lake light intensity in the growing season of Group 1 Isochrysidales (Yao et al., 2019). Higher light intensity under thinner lake ice (warmer winter temperatures) may trigger the earlier growth of Group I Isochrysidales even in the winter, possibly leading to a more sensitive response of the R3b to winter temperatures in the relatively warm regions (Yao et al., 2019).

In our sediment core, U^K_{37} values are strongly correlated with U^K_{38}Et (R^2 = 0.882; Fig. 8c), whereas R3b values have poor (but negative) correlations with U^K_{37} and U^K_{38}Et (R^2 = 0.056 and 0.205; Fig. 8a, b). We hypothesize that these differences among the correlations may mainly be contributed to different responses of these indices to seasonal

temperatures. During early spring growth season (early growth of Group 1 Isochrysidales; Longo et al., 2018) with relatively cold lake water temperatures, Group 1 Isochrysidales may respond to lake water temperatures at that time by primarily adjusting the ratio of two isomers $C_{38:3b}Et$ and $C_{37:3b}$. The lake temperature changes during the early spring growth season may depend on maximum lake ice thickness that is mainly determined by winter temperatures (Yao et al., 2019). This may, in part, explain our observed correlation between R3b and winter temperature from surface sediments of Northern Hemispheric freshwater lakes when the mean winter temperature is >~–20 °C (Yao et al., 2019). Whereas during the Group 1 bloom period of the spring transitional season with relatively warm lake water temperatures, Group 1 U^K_{37} and $U^K_{38}Et$ better record the lake water temperatures at that time (Longo et al., 2018; Yao et al., 2019). Further, we analyzed the correlations between spring and winter temperatures (1953–present) from the Arxan weather station near our study site. Winter temperatures show a positive correlation with spring temperatures (Supplementary Fig. S4). Thus, our observed negative correlations of R3b with U^K_{37} and $U^K_{38}Et$ in our sediment core cannot be fully explained by the potential different seasonality of these proxies.

Alternatively, the regional mean winter temperature in Tuofengling Tianchi is ~–21 °C (1979–2013; Yao et al., 2019), and R3b becomes relatively insensitive to the changes in the cold-season temperatures in such cold environment setting (Yao et al., 2019). The R3b proxy in our sediment core may be complicated by other unknown environmental variables. Further studies involving a systematic SPM sampling and lake water chemistry measurements in Tuofengling Tianchi throughout the Group 1 growth season may help explain such divergence of these temperature proxies in sediments.

4. Conclusions

We found genetic diversity in alkenone-producing Isochrysidales in a sediment core from Tuofengling Tianchi (freshwater volcanic lake) in northeastern China, with 11 ASVs all of which belong to Group 1 Isochrysidales. Consistent with DNA results, the LCA distributions display typical characteristic of Group 1 Isochrysidales-producing LCAs with RIK_{37} of 0.51–0.60. We divided 11 ASVs into two main subclades Groups 1a and 1b based on our reconstructed phylogenetic tree. Our combination of DNA and LCA results indicates that the LCA-based temperature proxies U^K_{37}, $U^K_{38}Et$, and R3b are not significantly affected by the variable mixtures of two Group 1 subclades. However, the reason for our observed poor correlations of R3b with U^K_{37} and $U^K_{38}Et$ in our sediment core may be further revealed by sampling a series of SPM and lake water samples of the freshwater volcanic lakes throughout a seasonal cycle of Group 1 Isochrysidales growth.

Declaration of Competing Interest

The authors declare that they have no known competing financial interests or personal relationships that could have appeared to influence the work reported in this paper.

Acknowledgments

This work was supported by the National Natural Science Foundation of China (No. 42073070; 41888101; 42130503). We thank J. Wu, K. Wang, and J. Zhao for assistance during field sampling and H. Du for the radiocarbon measurements. We are also grateful the comments from Dr. Ken Sawada and an anonymous reviewer, and editors Dr. John Volkman and Dr. Elizabeth Minor that helped us improve the manuscript.

Appendix A. Supplementary material

Supplementary data to this article can be found online at https://doi.org/10.1016/j.orggeochem.2022.104483.

References

Araie, H., Nakamura, H., Toney, J.L., Haig, H.A., Plancq, J., Shiratori, T., Leavitt, P.R., Seki, O., Ishida, K., Sawada, K., Suzuki, I., Shiraiwa, Y., 2018. Novel alkenone-producing strains of genus Isochrysis (Haptophyta) isolated from Canadian saline lakes show temperature sensitivity of alkenones and alkenoates. Organic Geochemistry 121, 89–103.

Bolyen, E., Rideout, J.R., et al., 2019. Reproducible, interactive, scalable and extensible microbiome data science using QIIME 2. Nature Biotechnology 37, 852–857.

Brassell, S.C., Brereton, R.G., Eglinton, G., Grimalt, J., Liebezeit, G., Marlowe, I.T., Pflaumann, U., Sarnthein, M., 1986. Palaeoclimatic signals recognized by chemometric treatment of molecular stratigraphic data. Organic Geochemistry 10, 649–660.

Callahan, B.J., McMurdie, P.J., Rosen, M.J., Han, A.W., Johnson, A.J.A., Holmes, S.P., 2016. DADA2: High-resolution sample inference from Illumina amplicon data. Nature Methods 13, 581–583.

Chen, S., Zhou, Y., Chen, Y., Gu, J., 2018. fastp: an ultra-fast all-in-one FASTQ preprocessor. Bioinformatics 34, i884–i890.

Chu, G., Sun, Q., Li, S., Zheng, M., Jia, X., Lu, C., Liu, J., Liu, T., 2005. Long-chain alkenone distributions and temperature dependence in lacustrine surface sediments from China. Geochimica et Cosmochimica Acta 69, 4985–5003.

Conte, M.H., Thompson, A., Lesley, D., Harris, R.P., 1998. Genetic and physiological influences on the alkenone/alkenoate versus growth temperature relationship in Emiliania huxleyi and Gephyrocapsa oceanica. Geochimica et Cosmochimica Acta 62, 51–68.

Conte, M.H., Sicre, M., Ruhlemann, C., Weber, J.C., Schulte, S., Schulz-Bull, D., Blanz, T., 2006. Global temperature calibration of the alkenone unsaturation index $U^{K'}_{37}$ in surface waters and comparison with surface sediments. Geochemistry Geophysics Geosystems 7, Q02005.

Coolen, M.J.L., Muyzer, G., Rijpstra, W.I.C., Schouten, S., Volkman, J.K., Sinninghe Damsté, J.S., 2004. Combined DNA and lipid analyses of sediments reveal changes in Holocene haptophyte and diatom populations in an Antarctic lake. Earth and Planetary Science Letters 223, 225–239.

D'Andrea, W.J., Lage, M., Martiny, J.B.H., Laatsch, A.D., Amaral-Zettler, L.A., Sogin, M. L., Huang, Y., 2006. Alkenone producers inferred from well-preserved 18S rDNA in Greenland lake sediments. Journal of Geophysical Research 111, G03013.

D'Andrea, W.J., Huang, Y., Fritz, S.C., Anderson, N.J., 2011. Abrupt Holocene climate change as an important factor for human migration in West Greenland. Proceedings of the National Academy of Sciences 108, 9765–9769.

D'Andrea, W.J., Theroux, S., Bradley, R.S., Huang, X., 2016. Does phylogeny control temperature sensitivity? Implications for lacustrine alkenone paleothermometry. Geochimica et Cosmochimica Acta 175, 168–180.

Egge, E., Bittner, L., Andersen, T., Audic, S., de Vargas, C., Edvardsen, B., 2013. 454 pyrosequencing to describe microbial eukaryotic community composition, diversity and relative abundance: A test for marine haptophytes. PLoS One 8, e74371.

Eglinton, G., Bradshaw, S.A., Rosell, A., Sarnthein, M., Pflaumann, U., Tiedemann, R., 1992. Molecular record of secular sea surface temperature changes on 100-year timescales for glacial terminations I, II, IV. Nature 356, 423–426.

Huang, Y., Zheng, Y., Heng, P., Giosan, L., Coolen, M.J.L., 2021. Black Sea paleosalinity evolution since the last deglaciation reconstructed from alkenone-inferred Isochrysidales diversity. Earth and Planetary Science Letters 564, 116881.

Kaiser, J., Wang, K.J., Rott, D., Li, G., Zheng, Y., Amaral-Zettler, L., Arz, H.W., Huang, Y., 2019. Changes in long chain alkenone distributions and Isochrysidales groups along the Baltic Sea salinity gradient. Organic Geochemistry 127, 92–103.

Karger, D.N., Conrad, O., Böhner, J., Kawohl, T., Kreft, H., Soria-Auza, R.W., Zimmermann, N.E., Linder, H.P., Kessler, M., 2017. Climatologies at high resolution for the Earth's land surface areas. Scientific Data 4, 170122.

Liao, S., Yao, Y., Wang, L., Wang, K.J., Amaral-Zettler, L., Longo, W.M., Huang, Y., 2020. C41 methyl and C42 ethyl alkenones are biomarkers for Group II Isochrysidales. Organic Geochemistry 147.

Longo, W.M., Dillon, J.T., Tarozo, R., Salacup, J.M., Huang, Y., 2013. Unprecedented separation of long-chain alkenones from gas chromatography with a poly (trifluoropropylmethylsiloxane) stationary phase. Organic Geochemistry 65, 94–102.

Longo, W.M., Theroux, S., Giblin, A.E., Zheng, Y., Dillon, J.T., Huang, Y., 2016. Temperature calibration and phylogenetically distinct distributions for freshwater alkenones: evidence from northern Alaskan lakes. Geochimica et Cosmochimica Acta 180, 177–196.

Longo, W.M., Huang, Y., Yao, Y., Zhao, J., Giblin, A.E., Wang, X., Zech, R., Haberzettl, T., Jardillier, L., Toney, J.L., Liu, Z., Krivonogov, S., Kolpakova, M., Chu, G., D'Andrea, W.J., Harada, N., Nagashima, K., Sato, M., Yonenobu, H., Yamada, K., Gotanda, K., Shinozuka, Y., 2018. Widespread occurrence of distinct alkenones from Group I haptophytes in freshwater lakes: implications for paleotemperature and paleoenvironmental reconstructions. Earth and Planetary Science Letters 492, 239–250.

Longo, W.M., Huang, Y., Russell, J.M., Morrill, C., Daniels, W.C., Giblin, A.E., Crowther, J., 2020. Insolation and greenhouse gases drove Holocene winter and spring warming in Arctic Alaska. Quaternary Science Reviews 242, 106438.

Magoč, T., Salzberg, S.L., 2011. FLASH: fast length adjustment of short reads to improve genome assemblies. Bioinformatics 27, 2957–2963.

Marlowe, I.T., Brassell, S.C., Eglinton, G., Green, J.C., 1990. Long-chain alkenones and alkyl alkenoates and the fossil coccolith record of marine sediments. Chemical Geology 88, 349–375.

Nakamura, H., Sawada, K., Araie, H., Suzuki, I., Shiraiwa, Y., 2014. Long chain alkenes, alkenones and alkenoates produced by the haptophyte alga Chrysotila lamellosa CCMP1307 isolated from a salt marsh. Organic Geochemistry 66, 90–97.
Pearson, E.J., Juggins, S., Farrimond, P., 2008. Distribution and significance of long-chain alkenones as salinity and temperature indicators in Spanish saline lake sediments. Geochimica et Cosmochimica Acta 72, 4035–4046.
Plancq, J., McColl, J.L., Bendle, J.A., Seki, O., Couto, J.M., Henderson, A.C.G., Yamashita, Y., Kawamura, K., Toney, J.L., 2018. Genomic identification of the long-chain alkenone producer in freshwater Lake Toyoni, Japan: implication for temperature reconstructions. Organic Geochemistry 125, 189–195.
Plancq, J., Couto, J.M., Ijaz, U.Z., Leavitt, P.R., Toney, J.L., 2019. Next generation sequencing to identify lacustrine haptophytes in the Canadian Prairies: significance for temperature proxy applications. Journal of Geophysical Research: Biogeosciences 124, 2144–2158.
Prahl, F.G., Wakeham, S.G., 1987. Calibration of unsaturation patterns in long-chain ketone compositions for palaeotemperature assessment. Nature 330, 367–369.
Richter, N., Longo, W.M., George, S., Shipunova, A., Huang, Y., Amaral-Zettler, L., 2019. Phylogenetic diversity in freshwater-dwelling Isochrysidales haptophytes with implications for alkenone production. Geobiology 17, 272–280.
Richter, N., Russell, J.M., Garfinkel, J., Huang, Y., 2021. Winter-spring warming in the North Atlantic during the last 2000 years: evidence from southwest Iceland. Climate of the Past 17, 1363–1383.
Sawada, K., Handa, N., Shiraiwa, Y., Danbara, A., Montani, S., 1996. Long-chain alkenones and alkyl alkenoates in coastal and pelagic sediments of the northwest North Pacific with special reference to the reconstruction of Emiliania huxleyi and Gephyrocapsa oceanica ratios. Organic Geochemistry 24, 751–764.
Sawada, K., Ono, M., Nakamura, H., Tareq, S.M., 2020. Reconstruction of Holocene Optimum paleoclimatic variations using long-chain n-alkanes and alkenones in sediments from Dabusu Lake, northeastern China. Quaternary International 550, 27–38.
Simon, M., López-García, P., Moreira, D., Jardillier, L., 2013. New haptophyte lineages and multiple independent colonizations of freshwater ecosystems. Environmental Microbiology Reports 5, 322–332.
Sun, Q., Chu, G., Liu, G., Li, S., Wang, X., 2007. Calibration of alkenone unsaturation index with growth temperature for a lacustrine species, Chrysotila lamellosa (Haptophyceae). Organic Geochemistry 38, 1226–1234.
Theroux, S., D'Andrea, W.J., Toney, J.L., Amaral-Zettler, L., Huang, Y., 2010. Phylogenetic diversity and evolutionary relatedness of alkenone-producing haptophyte algae in lakes: Implications for continental paleotemperature reconstructions. Earth and Planetary Science Letters 300, 311–320.
Theroux, S., Huang, Y., Toney, J.L., Andersen, R., Nyren, P., Bohn, R., Salacup, J., Murphy, L., Amaral-Zettler, L., 2020. Successional blooms of alkenone-producing haptophytes in Lake George, North Dakota: Implications for continental paleoclimate reconstructions. Limnology and Oceanography 65, 413–425.
Toney, J.L., Huang, Y., Fritz, S.C., Baker, P.A., Grimm, E., Nyren, P., 2010. Climatic and environmental controls on the occurrence and distributions of long chain alkenones in lakes of the interior United States. Geochimica et Cosmochimica Acta 74, 1563–1578.
Volkman, J.K., Eglinton, G., Corner, E.D.S., Forsberg, T.E.V., 1980. Long-chain alkenes and alkenones in the marine coccolithophorid Emiliania huxleyi. Phytochemistry 19, 2619–2622.
Volkman, J.K., Barrett, S.M., Blackburn, S.I., Sikes, E.L., 1995. Alkenones in Gephyrocapsa oceanica: implications for studies of paleoclimate. Geochimica et Cosmochimica Acta 59, 513–520.
Wang, K.J., O'Donnell, J.A., Longo, W.M., Amaral-Zettler, L., Li, G., Yao, Y., Huang, Y., 2019a. Group I alkenones and Isochrysidales in the world's largest maar lakes and their potential paleoclimate applications. Organic Geochemistry 138, 103924.
Wang, L., Longo, W.M., Dillon, J.T., Zhao, J., Zheng, Y., Moros, M., Huang, Y., 2019b. An efficient approach to eliminate steryl ethers and miscellaneous esters/ketones for gas chromatographic analysis for alkenones and alkenoates. Journal of Chromatography A 1596, 175–182.
Yao, Y., Zhao, J., Longo, W.M., Li, G., Wang, X., Vachula, R.S., Wang, K.J., Huang, Y., 2019. New insights into environmental controls on the occurrence and abundance of Group I alkenones and their paleoclimate applications: Evidence from volcanic lakes of northeastern China. Earth and Planetary Science Letters 527, 115792.
Yao, Y., Lan, J., Zhao, J., Vachula, R.S., Xu, H., Cai, Y., Cheng, H., Huang, Y., 2020. Abrupt freshening since the early Little Ice Age in Lake Sayram of arid central Asia inferred from an alkenone isomer proxy. Geophysical Research Letters 47 e2020GL089257.
Yao, Y., Huang, Y., Zhao, J., Wang, L., Ran, Y., Liu, W., Cheng, H., 2021. Permafrost thaw induced abrupt changes in hydrology and carbon cycling in Lake Wudalianchi, northeastern China. Geology 49, 1117–1121.
Yao, Y., Zhao, J., Vachula, R.S., Liao, S., Li, G., Pearson, E.J., Huang, Y., 2022. Phylogeny, alkenone profiles and ecology of Isochrysidales subclades in saline lakes: Implications for paleosalinity and paleotemperature reconstructions. Geochimica et Cosmochimica Acta 317, 472–487.
Zheng, Y., Huang, Y., Andersen, R.A., Amaral-Zettler, L.A., 2016. Excluding the di-unsaturated alkenone in the U^{K}_{37} index strengthens temperature correlation for the common lacustrine and brackish-water haptophytes. Geochimica et Cosmochimica Acta 175, 36–46.
Zheng, Y., Heng, P., Conte, M.H., Vachula, R.S., Huang, Y., 2019. Systematic chemotaxonomic profiling and novel paleotemperature indices based on alkenones and alkenoates: potential for disentangling mixed species input. Organic Geochemistry 128, 26–41.
Zink, K., Leythaeuser, D., Melkonian, M., Schwark, L., 2001. Temperature dependency of long-chain alkenone distributions in Recent to fossil limnic sediments and in lake waters. Geochimica et Cosmochimica Acta 65, 253–265.